Fluorescence polarization reveals a possible displacement model of competition in PRC2:RNA:DNA interactions

Regan Fenske

Department of Molecular, Cellular, and Developmental Biology

Thesis Advisor:

Dr. Thomas Cech (BCHM/MCDB)

Committee Members:

Dr. Christy Fillman (MCDB)

Dr. Jiyhe Park (CHEM)

University of Colorado, Boulder

Defense: October 28, 2022

Abstract

PRC2 is a histone methyltransferase that acts on histone subunit H3 at lysine 27 to repress chromatin state and inhibit gene expression. The interactions between PRC2 and RNA have been heavily studied *in vivo* and *in vitro* with conflicting results reported on the relationship, but there is less data on interactions between PRC2 and DNA. Fluorescence polarization-based methodology was used with various RNA and DNA species to study the binding kinetics of PRC2 with RNA and DNA. Previous data indicate that PRC2 has a relatively high affinity for DNA species that are rich in consecutive G and C nucleotides. Double-stranded DNA species with lengths of 50-60 bp were designed for this project. Fluorescence polarization binding experiments were used to identify the general binding affinity of the DNA and RNA species to PRC2 by calculating the K_d apparent for the binding curve. After the apparent binding affinities were determined, various FP-competition experiments were performed to determine if each DNA species could be competed off by an RNA species or itself, and vice versa. These results showed that the DNA species were more effective competitors although the RNA species were stronger binders. These results suggest a mechanism for RNA-mediated PRC2 regulation that could reconcile the conflicting experimental results and interpretations of past experiments. Further FP-based K_d experiments under varying salt concentrations revealed PRC2 has ionic interactions with DNA that are not seen with RNA. This suggests PRC2 has extra unique interactions with DNA, which could explain the differing effectiveness of DNA versus RNA as competitors. Altogether, the results imply that DNA has additional contacts with PRC2 that limit its displacement by RNA, allowing for RNA to guide PRC2 to its target genetic loci and then for PRC2 to deposit its methyl marks without being sequestered by RNA.

Table of Contents

Background

Polycomb Repressive Complex 2

Structure of PRC2

Polycomb Repressive Complex 2 (PRC2) is a histone methyltransferase (HMTase) that deposits three methyl groups onto lysine 27 of histone H3 (H3K27me1/2/3) (Fig. 1a). It was previously known that Polycomb group proteins maintain transcriptional repression during development. It was hypothesized that the PRC2 complex could create repressive chromatin states by methylation, which led to the identification of PRC2 as an HMTase for the specific mark of lysine 27 on histone H3 (Czermin, B. et al. 2002; Müller, J. et al. 2002; Kuzmichev, A. et al. 2002).

The core protein of PRC2 is made up of 4 subunits including EZH2, SUZ12, EED, and RBBP4. The SUZ12 conserved gene and EED/EZH protein complex were both associated with Polycomb group proteins in 2001 (Birve, A. et al. 2001; Satijn, D. P. et al. 2001). RbAp48, also known as RBBP4, is a mammalian homologue of Nurf55 and was associated with the complex of PRC2 in 2005 (Nekrasov, M. 2005). SUZ12 is the scaffold subunit which, along with its associated proteins, drives the association of PRC2 with chromatin (Youmans, D. T. et al. 2018). EZH2 contains the HMTase SET domain and is responsible for the trimethylation of H3K27 (Wang, X. et al. 2019). EED and RBBP4 act as the histone tail-binding subunit and histone chaperone subunit, respectively, and enhance the methyltransferase activity of EZH2. PRC2 also has cofactors which help to regulate PRC2's methyltransferase activity. AEBP2, one such cofactor, has been shown to stimulate PRC2's HMTase activity in vitro (Grijzenhout, A. et al. 2016). AEBP2 exists in two major isoforms, (1) a short (32 kDa) embryonic form, and (2) a long

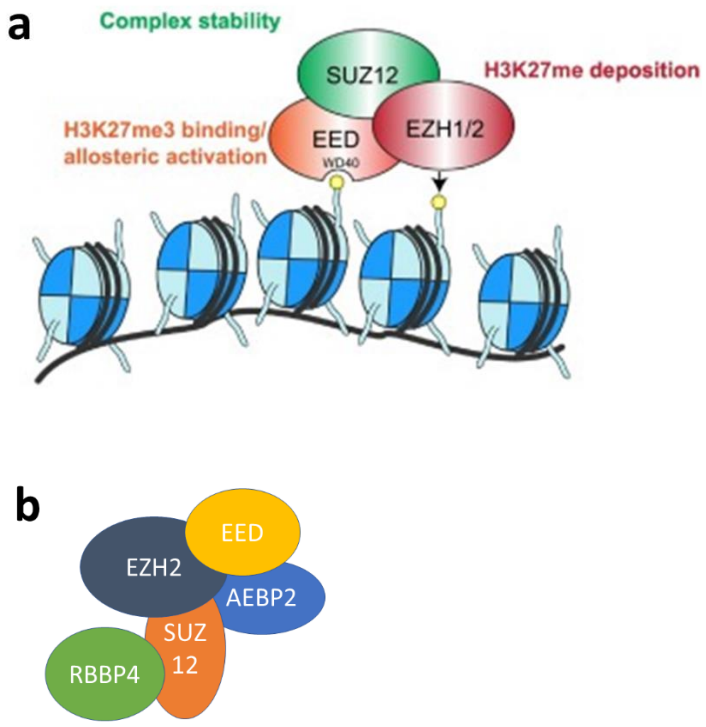

Figure 1. Structure of PRC2

(a) Three of the four core subunits of PRC2 are involved in methyltransferase activity. SUZ12 stabilizes the complex while EED and EZH1/2 bind to the nucleosome DNA and deposit the three methyl groups respectively (From Mierlo et. al, 2019).

(b) A representation of the five subunits comprising the PRC2 5m complex with the four core subunits and the additional AEBP2 subunit. AEBP2 exists in two isoforms, the short or long isoform. The complex used in this paper was the short form.

(52 kDa) somatic form (Kim, H. et al. 2015). The 5 subunit PRC2 complex with the short form of AEBP2 is the primary protein studied in this paper (Fig. 1b).

Biological relevance

PRC2's main function as an HMTase enzyme is to regulate DNA by suppressing gene expression. PRC2's activity is crucial for epigenetic silencing during embryonic development, cell differentiation, and cancer. In embryonic stem cells, PRC2 binds active promoters and methylates genes with both active and repressive marks at the same location (Kaneko, S. et al. 2013). PRC2 has a crucial silencing role at these genetic loci which influences their cell-fate decision (Di Croce, L., & Helin, K. 2013). If PRC2 is inactivated at any of these loci, the stem

cells can undergo differentiation, like during the formation of the epidermis for example (Margueron, R., & Reinberg, D. 2011). Disrupted regulation of PRC2 has been linked with various diseases such as melanoma, lymphoma, breast, and prostate cancers. One component of PRC2, EZH2, has been reported to be a factor in the more aggressive stages of prostate and breast cancer. Other components of PRC2 have been experimentally linked to increased cell proliferation as well (Margueron, R., & Reinberg, D. 2011).

Due to the crucial role of PRC2 during development and cancer, the mechanism by which it is targeted to specific genetic loci is of great interest. Polycomb group (PcG) complexes in general have been shown to bind long noncoding RNAs (lncRNAs) and CpG islands, which have been proposed to target them to genetic loci (Simon, J. A., & Kingston, R. E. 2013).

PRC2 and RNA kinetics

The relationship of PRC2 and RNA has been heavily researched given PRC2's promiscuous binding to RNA transcripts (Davidovich, C. et al. 2013, 2015). Like the PcG complexes mentioned before, PRC2 interacts specifically with lncRNAs and pre-mRNAs in cells (Davidovich, C., & Cech, T. R. 2015). PRC2 has also shown a high affinity for G-tract motifs *in vivo*, specifically G-quadruplex structures, which are ubiquitous in the human transcriptome (Fig. 2). This supports the current view that PRC2 is regulated by the binding of G-tract-containing nascent RNA, including lncRNAs and pre-mRNAs (Wang, X. et al. 2017, 2019).

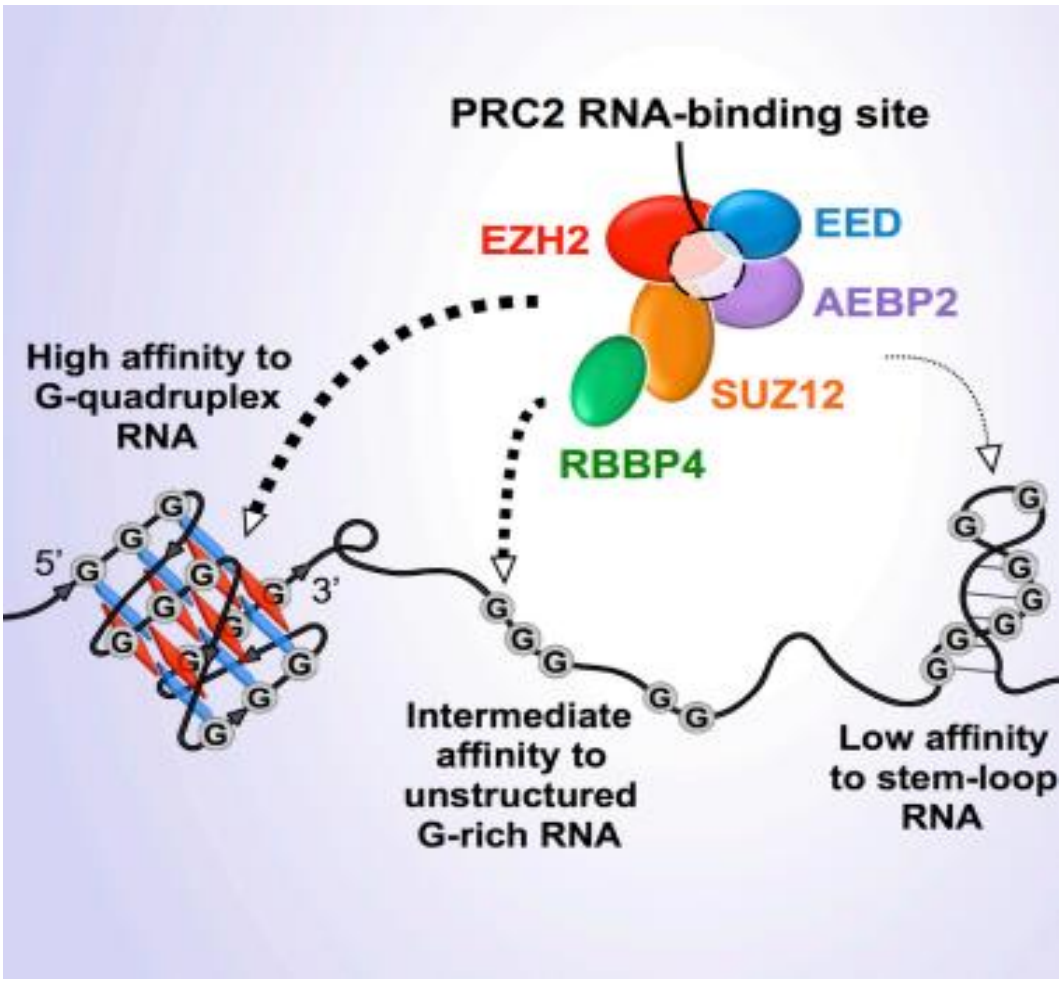

Figure 2. PRC2 binding affinities to RNA species

PRC2 5mer long form showed a higher binding affinity to G-quadruplex forming RNA than to other forms of RNA. Unstructured G-rich RNA and stem-loop forming RNA showed lower affinity to PRC2. (From Wang, X. et al. 2016).

However, the nature of how RNA regulated the HMTase activity of PRC2 differed *in vivo* and *in vitro*. The Wang et al. (reference) concluded that RNA inhibits the activity of PRC2 by sequestering it from nucleosome substrates *in vitro*. They theorized that RNA and DNA binding to PRC2 was mutually exclusive, so RNA could sequester PRC2 from the nucleosome substrates since PRC2 needs linker DNA to bind (Wang, X. et al. 2017). These findings were

consistent with various papers showing how RNA antagonistically regulates the enzymatic activity of PRC2 by inhibiting EZH2's catalytic activity (Kaneko, S. et al. 2014; Zhang, Q. et al. 2019; Cifuentes-Rojas, C. et al. 2014; Beltran, M. et al. 2016).

Interestingly, the Long et al. (reference) found that RNA was required for PRC2 localization to target genes *in vivo*. They proposed two models of how RNA regulates PRC2: (1) model one, that RNA recruits PRC2 to the chromatin, and/or (2) model two, that RNA evicts PRC2 from the chromatin (Long, Y. et al. 2020). These contradictory findings sparked the question of how to reconcile these findings *in vitro* and *in vivo*.

Current Project

Potential model of displacement ("Hand-Off" Model)

As mentioned before, the Wang et al. (reference) found that RNA and DNA binding to PRC2 was mutually antagonistic as they need to compete for the same or overlapping binding spots. The accepted model of ligand transfer with PRC2 has been that when the enzyme is bound to one polynucleotide species, any other polynucleotide is unable to associate with the protein until the first one dissociates. This classic competition model has mostly been applied to studies under conditions without considering *in vivo* elements, using RNA in free solution rather than the state of the chromatin-associated nascent RNA most likely involved in PRC2 regulation.

Wayne Hemphill proposed a model of displacement referred to as the "Hand-Off" Model, wherein PRC2 has the ability to "hand-off" one nucleic acid for another without completely dissociating from the first. Under the assumptions of this model, PRC2 would quickly form an extremely unstable intermediate complex with two nucleic acid substrates partially bound at the

same time. This model of competition could reconcile the contradictory findings of the previous studies. We sought to test this hypothesis by measuring the kinetics of PRC2, RNA, and DNA binding in experimental conditions resembling *in vivo* conditions.

Fluorescence Polarization

To measure the kinetics of PRC2, RNA, and DNA binding and competition, fluorescence polarization (FP) was used. Briefly, fluorescence polarization measures the emission light from a fluorescently labeled molecule after it is excited. Excitation light is passed though a polarizing filter onto the molecule in solution. The emission light coming off of the solution passes through two polarizing filters, (1) one parallel to the excitation filter, and (2) one perpendicular to the filter. The light's apparent intensity drops depending on how much the molecule is rotated relative to the emission filters due to the excitation-emission delay of the molecule, so the speed at which the molecule was rotating can be gathered from the intensities through the two emission filters (Fig. 3a).

For these experiments, the molecule in solution was a fluorescently labeled oligo with a varying concentration of enzyme. If an oligo is bound to a unit of enzyme, its rotation will be slower than the rotation of a free oligo, so the emission light values will be different for bound and unbound nucleic acids. The measurements of the parallel and perpendicular fluorescence intensity values detected relative to the direction of the polarized excitation light can then be calculated and expressed as a relative polarization value in units of milli polarization (mP) which can then be plotted as a function of varying enzyme concentration. At minimal enzyme

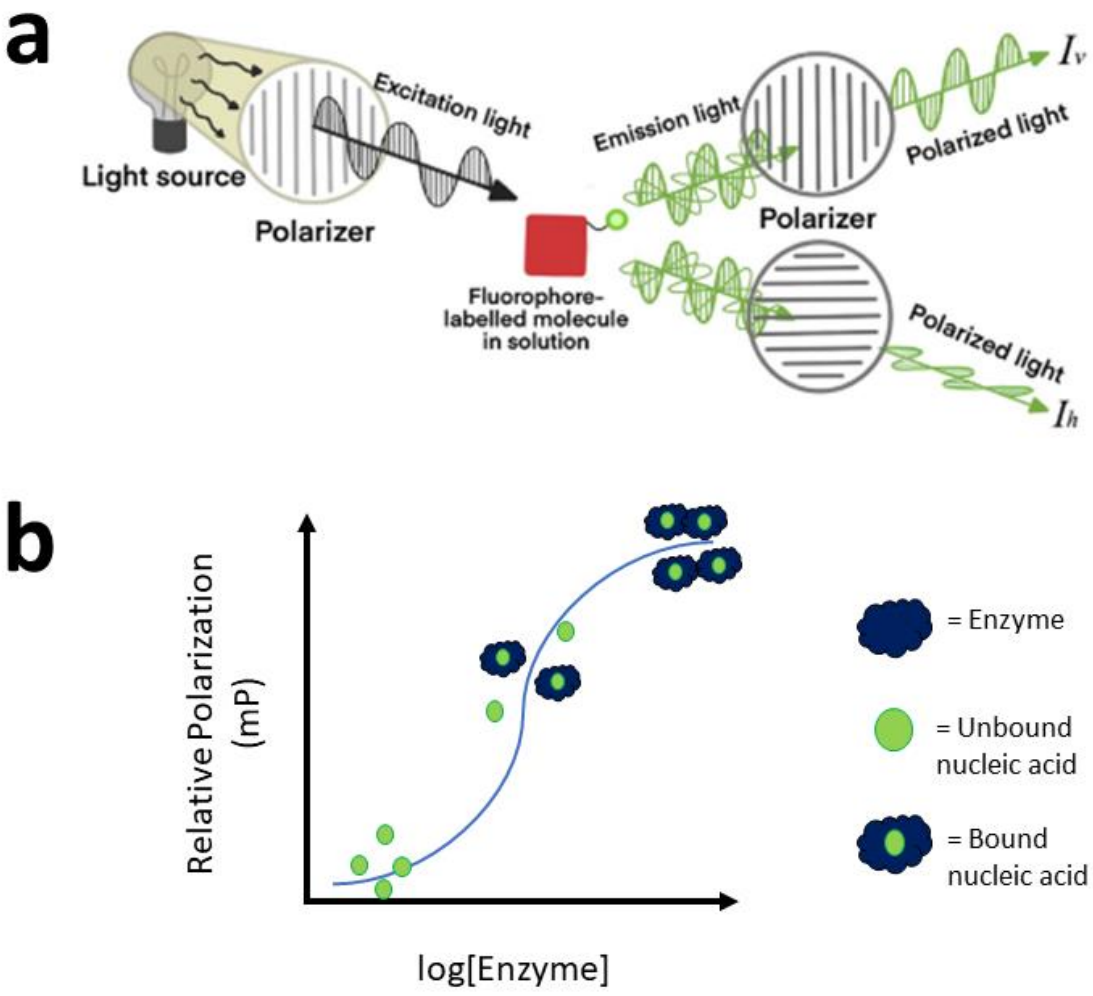

Figure 3. Fluorescence polarization schematic

(a) A light source goes through a polarizer and hits the fluorophore-labeled molecule in solution. The emission light from the fluorophore goes through two polarizer filters perpendicular to each other (From Zhao et al., 2020).

(b) The parallel and perpendicular values are normalized to relative mP values. The relative mP values from different time points are averaged and plotted as a function of log10 enzyme concentration. As the enzyme concentration increases, the amount of bound nucleic acid increases until maximum free enzyme levels are reached.

concentration, all the nucleic acids will be unbound, and at maximal enzyme concentration, the nucleic acid should all be bound (Fig. 3b).

This methodology used for FP-based binding experiments can also be used for competition experiments with two competing nucleic acid species, one fluorescently labeled 'prey' oligo and one unlabeled 'decoy' oligo. For the competition experiment, the fluorescently labeled prey and enzyme were pre-incubated to get fully bound nucleic acid. The unlabeled decoy was then added at varying concentrations. For the two models, different rate constants were calculated to explain the mode of competition (Fig. 4). For the classic model, the fluorescently labeled prey would dissociate from the enzyme leaving it free for the unlabeled decoy to associate. The "Hand-Off" (displacement-transfer) model would have the decoy oligo kicking off and replacing the prey oligo on the enzyme, in addition to intrinsic dissociation.

Oligo design

To test the competition of RNA and DNA in terms of PRC2 binding, the oligos were designed based on those present *in vivo* (Table 2). The G-quadruplex species used predominantly in this paper, $r(G_3A_2)_4$, forms a stable G-quadruplex structure which has been shown to bind to PRC2 with high affinity. PRC2 has also been shown to have a higher affinity for CG-rich regions of DNA (Wang, X. et al. 2016). CpG islands within certain loci are crucial for the recruitment of PRC2, so a DNA sequence rich in C and G base pairs was needed (Mendenhall, E. et al. 2010).

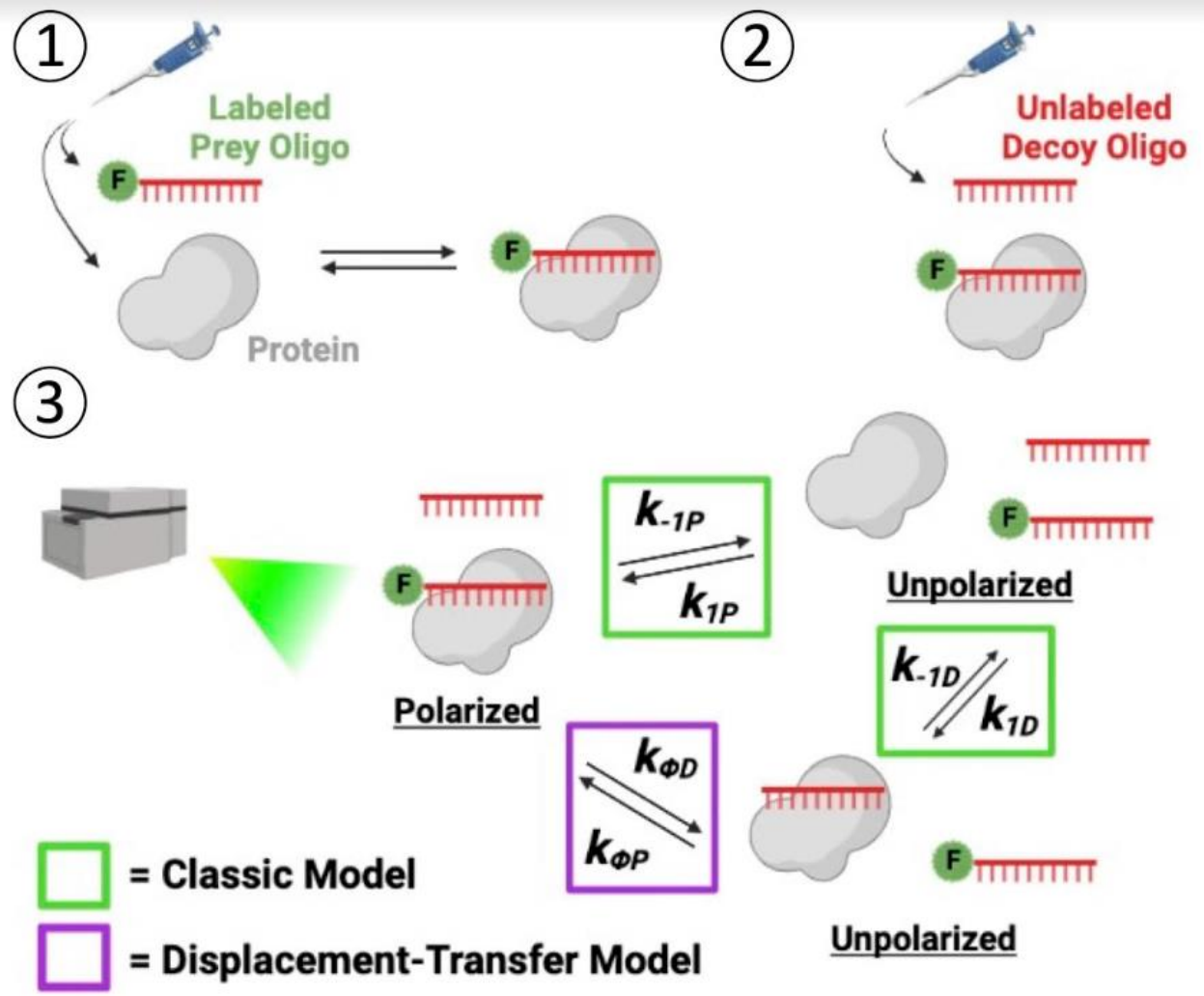

Figure 4. FP-Competition schematic for different models of nucleic acid competition

The competition experiment pre-incubates the fluorescently labeled oligo and enzyme to get fully bound nucleic acid then adds in an unlabeled oligo at varying concentrations.

The classic model, outlined in green, involves the fluorescently labeled oligo dissociating from the enzyme (with dissociation value k_{-1P}) and the unlabeled oligo associating with the enzyme (with association value k_{1D}), and vice versa.

The displacement-transfer model, outlined in purple, involves the unlabeled oligo replacing the fluorescently labeled oligo on the enzyme (with association value $k_{\Phi D}$), and vice versa.

Nucleosome linker DNA (20-60 bp long) is a necessary component in the PRC2-nucleosome interaction, so DNA species of lengths 50 and 60 bp were designed to mimic the interaction with PRC2 *in vivo* (Wang, X. et al. 2017). An oligo species with a randomized CG-rich sequence of 5 bp repeated 10 times (50 bp total) was designed. A second oligo species was created with a completely randomized CG-rich sequence with a slightly longer length of 60 bp. This species most closely resembles the DNA that PRC2 would target in the body. Both sequences were put through a software which predicts the likelihood of secondary structure formation, like hairpins or other intermolecular interactions. Neither were predicted to form any secondary structures, but this was not tested experimentally, so formation of secondary structures could be a factor.

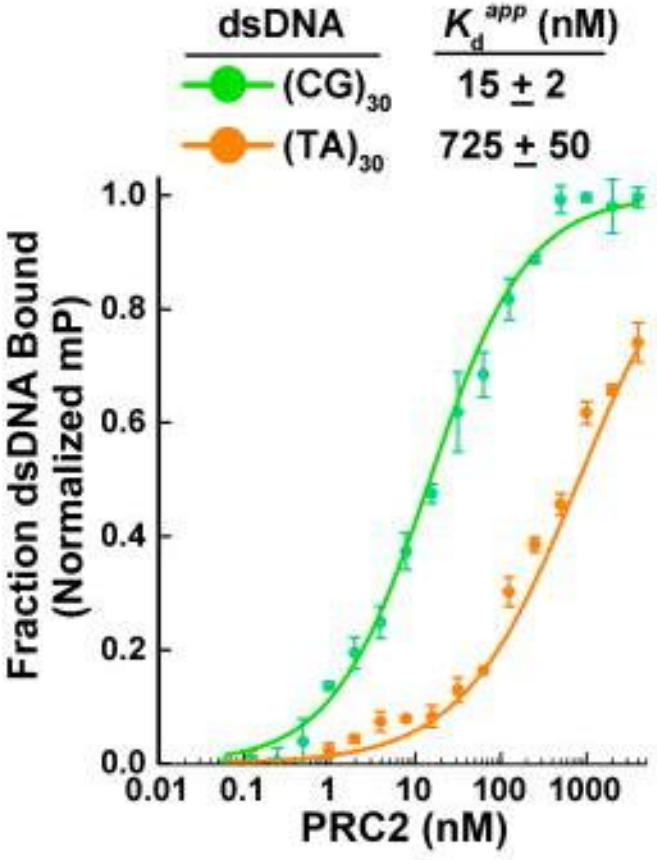

Figure 5. ds(CG)30 bound to PRC2 with a high affinity

An FP-based experiment was run with fluorescently labeled double-stranded DNA species and PRC2 5mer long form. PRC2 had a strong binding affinity to the ds(CG)30 species with a K_d apparent of 15 nM (From Wang et al., 2017).

Results

Competition kinetics of GCrich DNA and Gquad RNA

PRC2 Shows Strong Binding Affinity to Gquad RNA species and dsCG-rich DNA species

To confirm the expected relationship between the G-quadruplex RNA species and PRC2, an FP-based binding experiment was run with fluorescently labeled rG4-20 in low-salt and mid-salt buffer conditions (Table 1). The mid-salt buffer, at 25 mM KCl, was used to match the conditions in previous experiments testing a similar species (Wang, X. et al. 2017). The low-salt buffer, at 10 mM KCl, was tested to see if binding affinity could be increased with a lower salt. There was no difference in the binding affinity of rG4-20 to PRC2 between the two buffer conditions (Fig. 6a). To recapitulate the experiment that launched this project, an FP-competition experiment was run with fluorescently labeled rG4-20 as the prey and the same species unlabeled as the decoy in both low-salt and mid-salt buffer conditions (Fig. 6b). Similar to the FP-based binding experiment, the buffer conditions did not change the behavior. The regression statistics were calculated for all experiments (Fig. 6c). The apparent K_d of the rG4-20 was ~5 nM for both buffer conditions, which indicated high binding affinity with PRC2 and confirmed previous data with this oligo. Both competition experiments favored the 'hand-off' model, confirming previous data from Wayne Hemphill.

After designing the DNA oligos, we ran an FP-based experiment for each species to ensure they bind to PRC2 with relatively high affinity. An FP-based experiment was run in low-salt and mid-salt buffer conditions with fluorescently labeled dsCG-50 DNA species (Fig. 7a) and dsCG-60 DNA species (Fig. 7b). Originally, each oligo was only run in the mid-salt buffer

conditions, which yielded no binding to PRC2. The species were then run in the low-salt condition which

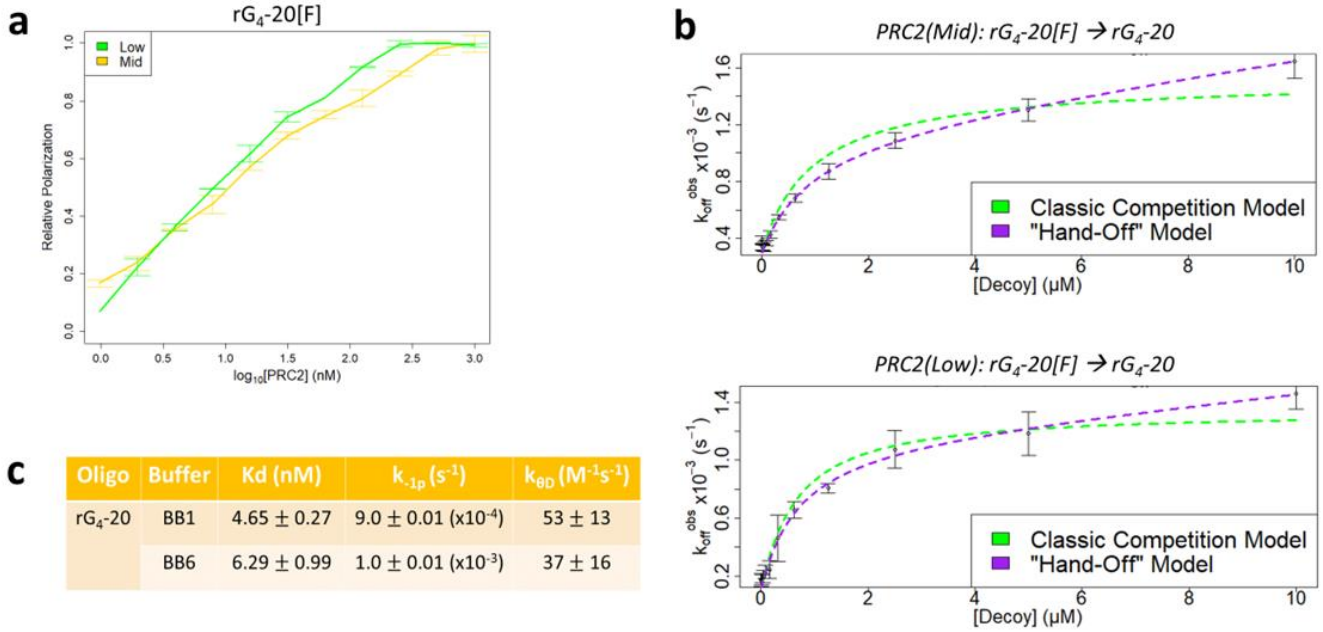

c

Oligo	Buffer	Kd (nM)	k_{-1p} (s^{-1})	$k_{\theta D}$ ($M^{-1}s^{-1}$)
rG_4-20	BB1	4.65 ± 0.27	9.0 ± 0.01 ($x10^{-4}$)	53 ± 13
	BB6	6.29 ± 0.99	1.0 ± 0.01 ($x10^{-3}$)	37 ± 16

Figure 6. PRC2 exhibits a strong binding affinity to G-quadruplex RNA, but the RNA is a weak competitor and displacer regardless of salt concentration.

(a) An FP-based binding experiment was done with the short 5mer PRC2 protein binding to G-quad RNA species in low-salt and mid-salt concentration.

(b) An FP-Competition was done at 4C using a fluorescently labeled G-quad RNA species as the prey and an unlabeled version of that species as a decoy in both low-salt and mid-salt conditions.

(c) The binding affinity of PRC2 was unchanged with the varying salt concentrations, shown by the near-identical K_d values calculated by the regression statistics. The competition dissociation of G-quad RNA from PRC2 was similarly unaffected by the varying salt concentrations.

improved the binding affinity to PRC2 significantly. The regression statistics were calculated for the FP-based experiments (Fig. 7c). The apparent Kd of each species in the mid-salt buffer were extremely high (the Kd values in the table were calculated to fit the regression statistics, so the

actual K_d apparent is much greater than the greatest enzyme concentration used) which indicates no binding. However, the apparent K_d of each species in the low-salt was ~4-5 nM, which is

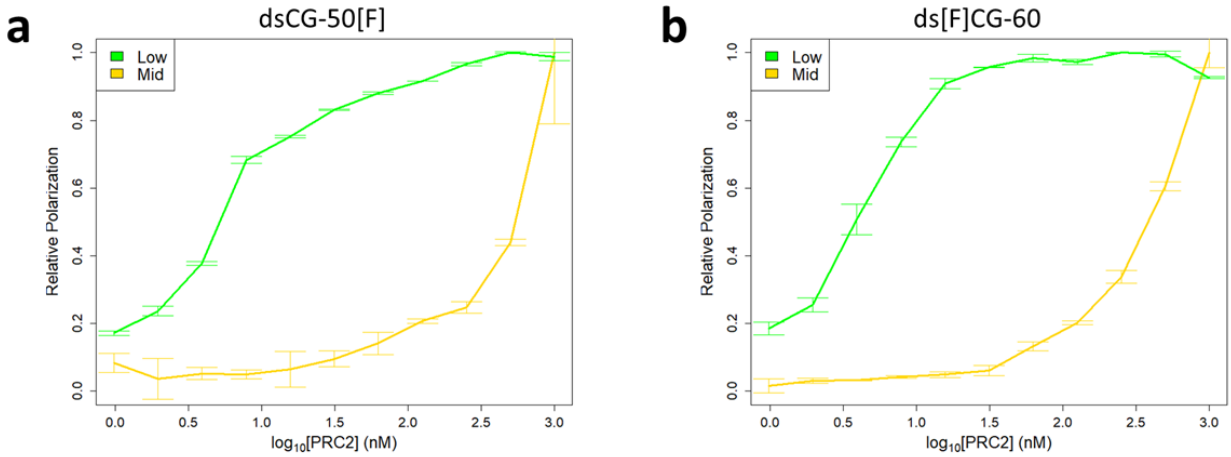

c

Oligo	Buffer	Kd
dsCG-50	BB1	3.04e6 ± 1.85e11*
	BB6	4.95 ± 0.46
dsCG-60	BB1	2.15e3 ± 1.26e3*
	BB6	3.45 ± 0.43

Figure 7. PRC2 shows a higher binding affinity to both dsCG-50 and dsCG-60 species with a lower salt concentration.

(a) An FP-based binding experiment was done with the short 5mer PRC2 protein binding to dsCG-50 DNA species and (b) dsCG-60 DNA species.

(c) The K_d values calculated from the regression statistics show a higher binding affinity to PRC2 in the low-salt concentration of BB6.

* These K_d values were calculated to fit the regression statistics and are not accurate representations of the K_d values for each oligo species.

comparable to the Kd of the rG4-20 species, so both DNA species were safe to continue with experimentation in the low-salt buffer.

PRC2 Showed Direct Transfer Between Gquad RNA and dsDNA species

Once we confirmed that PRC2 did indeed exhibit 'hand-off' behavior with two RNA species, we wanted to test the model with RNA and DNA. We ran four FP-competition reactions with the rG4-20 and the dsCG-60 species with every combination of prey and decoy as indicated (Fig. 8a). The results showed that every species exhibited the 'hand-off' behavior, but the dissociation values calculated for each experiment indicated differing levels of efficiency (Fig. 8b). In the RNA(prey)/DNA(decoy) experiment, the 'hand-off' rate constant ($k_{\theta D}$) for the DNA was more efficient relative to the RNA's prey dissociation rate constant (k_{-1P}) than the inverse experiment. These results indicate that the DNA species was better able to 'kick off' the RNA species from PRC2 than vice versa.

We also ran four FP-competition reactions with the rG4-20 and the dsCG-50 species to confirm these findings with another CG-rich DNA species (Supp. Fig. 8a-b). The data for these experiments were run under different conditions (as indicated in the figure legend) as the results differed for the conditions of the dsCG-60 species. Although the data did not look as favorable as the 60 bp data, the experiments were reconcilable. When tested under the same conditions as dsCG-60, the DNA/DNA experiment had some unfavorable escalation that led to regression artifacts that favored the classic model when the data should have favored the hand-off model. Although the results were reconcilable, the conditions could have acted as a possible extraneous factor resulting in the discrepancy between results. Regardless, the dsCG-60 species yielded interesting results backed up by the inclusion of the dsCG-50 species.

a

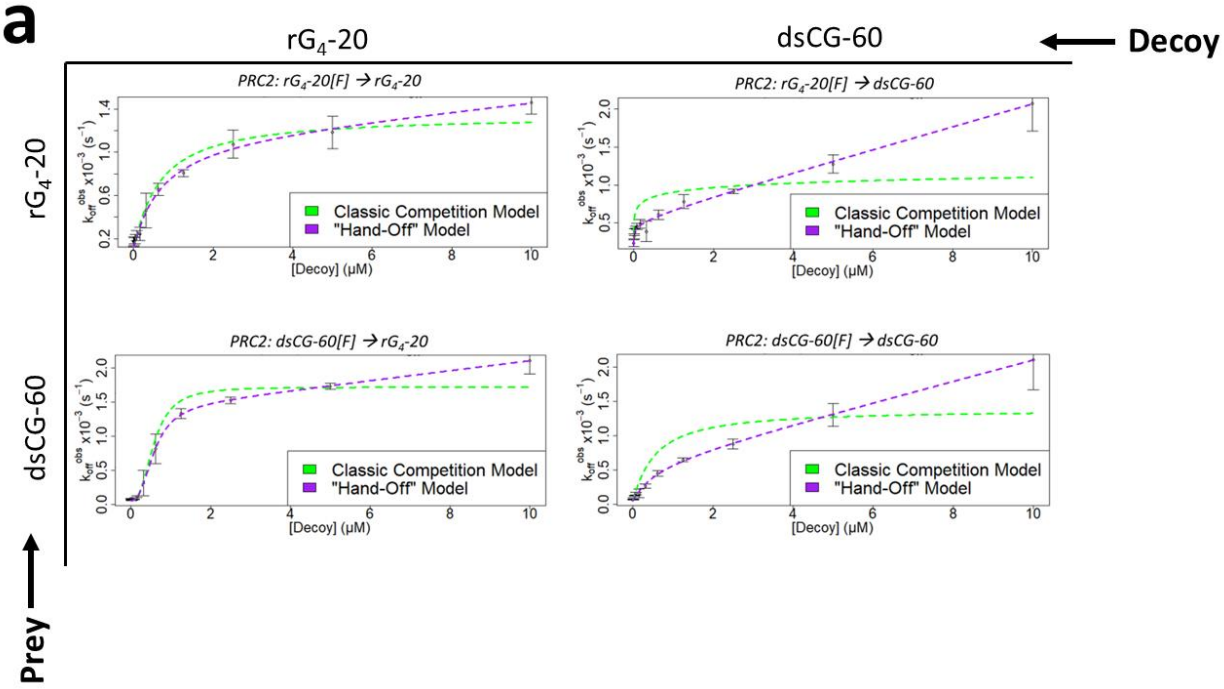

b

Prey	Decoy	k_{-1p} (s^{-1})	$k_{\theta D}$ ($M^{-1}s^{-1}$)
rG_4-20 [F]	rG_4-20	1.0 ± 0.01 ($x10^{-3}$)	37 ± 16
rG_4-20 [F]	dsCG-60	6.3 ± 2.1 ($x10^{-4}$)	150 ± 26
dsCG-60 [F]	rG_4-20	1.2 ± 0.06 ($x10^{-3}$)	67 ± 9
dsCG-60 [F]	dsCG-60	5.3 ± 2.3 ($x10^{-4}$)	150 ± 21

Figure 8. PRC2 Exhibits the "Hand-Off" Kinetics for Competition Dissociation with dsCG-60 and G-quadruplex RNA.

(a) FP-Competition experiments were run with combinations of G-quad RNA and dsCG-60 DNA as prey and decoy as labeled. All experiments were run at 4C with low-salt buffer conditions.

(b) Each combination of prey and decoy favored the "Hand-Off" Kinetic model, but the competition dissociation values calculated by regression statistics differed for each experiment.

Salt-dependent affinities of GCrich DNA and Gquad RNA for PRC2

dsDNA Species Show Different Salt-Dependent Affinities to PRC2 Not Seen with G-quad RNA

As mentioned before, prior studies have shown that RNA and DNA are mutually antagonistic with PRC2 binding, which suggests that there is competition for shared protein-polynucleotide contacts on PRC2 with the 'hand-off' model of displacement (Zhang, Q. et al. 2019). Both oligos had similar binding affinity to PRC2 (Fig. 6a and Fig. 7b), so the 'hand-off' kinetics should be similar between the oligos. However, as seen with the competition results, the kinetics for DNA displacing RNA are stronger than for RNA displacing either DNA or RNA. This suggests that there could be more contacts that are unique to either oligo influencing the kinetics.

To test this hypothesis, we ran FP-based binding experiments for the rG4-20 and dsCG-60 species with a range of buffer conditions to determine their K_d apparent at each salt concentration (Fig. 9a). The affinity of the rG4-20 to PRC2 was not affected by the salt concentration, with a similar K_d apparent for each buffer condition. The dsCG-60 however was greatly affected by the salt concentration, with wildly different K_d apparent values for each buffer. These results suggest that PRC2 has additional ionic contacts with dsDNA that it does not have with G-quadruplex RNA.

Once we confirmed the additional ionic contacts with dsDNA, we were curious if PRC2 also exhibited these unique contacts with single-stranded DNA. A single-stranded DNA oligo with a CG-rich 40nt long sequence was designed for this experiment. After we confirmed the oligo had a relatively strong binding affinity to PRC2, comparable to the dsDNA species (data not shown), the same experiment was performed under the Mid, High, and Very High buffer

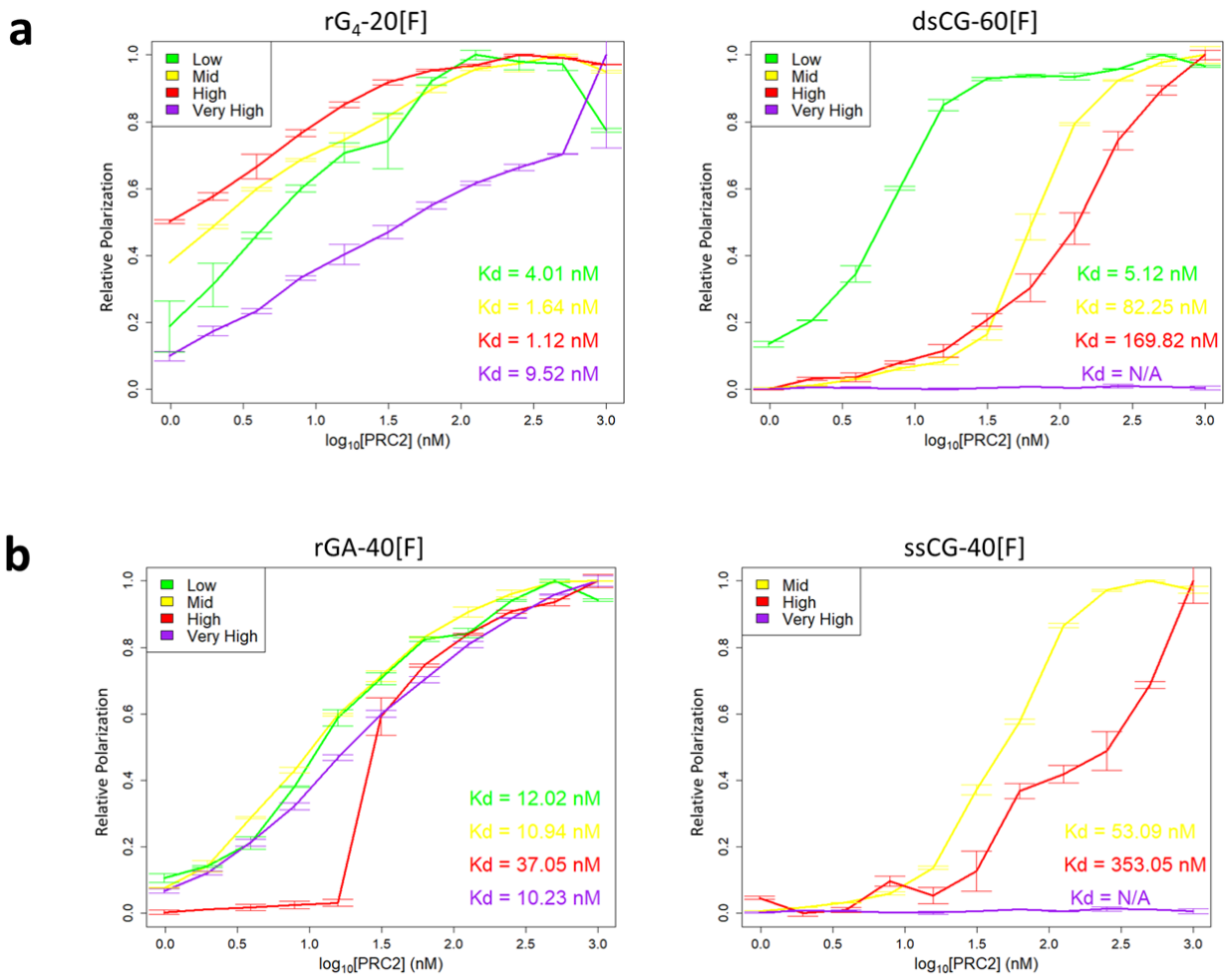

Figure 9. DNA species show salt-dependent affinity to PRC2 while RNA species are unaffected by the salt concentration.

FP-based binding experiments were run with four buffer conditions ranging from low-salt at 10mM KCl to very high-salt at 200mM KCl. Polarization values were normalized and plotted against each other with the K_d apparent values listed in the lower right-hand corner.

(a) G-quad RNA and dsCG-60 DNA were run with the varying salt concentrations.

(b) Unstructured RNA and ssCG-40 DNA were run with the varying salt concentrations, the ssCG-40 species was only run with the higher salt concentrations to confirm the difference in the higher variations.

conditions (excluding the low-salt condition to conserve materials). We were mostly curious to see if the higher salt concentrations (high-salt and very-high salt) would show the same variation as the dsDNA species. We also wanted to test an RNA species that would not form a G-quadruplex structure to see if an unstructured RNA could be influenced by the ionic contacts (Fig. 9b). The ssDNA species was shown to be salt-dependent, which could indicate that PRC2 forms ionic contacts with DNA regardless of if the species is single or double-stranded. The rGA-40 species was not salt-dependent, but interestingly had a much higher affinity than previous data suggested, although these experiments used a different form of PRC2.

Theoretical Reaction Simulations

Method

One crucial element of PRC2 interacting with DNA and RNA that has not been considered for these experiments yet is the methylation activity of PRC2 on nucleosomes. The point of studying PRC2's interactions as of yet has been in the ultimate interest of its activity in vivo. However, looking at the methylation activity of PRC2 on nucleosomes was not possible experimentally at the time. To be able to predict what these experiments could look like, Wayne Hemphill designed a custom script in RStudio (v.4.1.1) that would account for the extra variable of proximity. By adding this extra variable of the proximity of nucleosomes to nascent RNA, these simulations allow for the binding and consequent methylation activity of PRC2 on nucleosomes to be predicted under different conditions. These experiments consider the proximity to nascent RNA as well as the competition for binding between RNA and DNA, showing how these elements could affect PRC2's activity.

PRC2's 'Hand-Off' Kinetic Model Could Allow RNA-Mediated Recruitment to Nucleosomes

As previously mentioned, the discrepancy between RNA's roles *in vitro* and *in vivo* is still present. This issue raises the question if RNA can have antagonistic binding to PRC2 and yet still have a positive effect on the activity of the protein. To look more at the relationship with RNA and PRC2 in the cell, we simulated theoretical reactions that mimic PRC2's biochemical activity *in vivo* considering the proximity of nucleosomes and nascent RNA (Supp. Fig. 9). To simulate the reactions, we used the kinetic constants previously determined for each interaction and a new variable (α) which represents the effective molarity changes due to this RNA-nucleosome proximity (Fig. 10). These results indicate that in free solution (α = 1), RNA acts antagonistically towards PRC2's methyltransferase activity, as shown by the decrease in H3K27me3 marks as the RNA-nucleosome ratio increases. However, as the RNA-nucleosome proximity increases, mathematically shown by α increasing, RNA begins to act more synergistic. At these higher α levels, as the RNA-nucleosome ratio increases, the H3K27me3 marks are also increased.

These reaction schemes were dependent on 'hand-off' kinetics, which raises the question if RNA could still act synergistically if those were no longer in place. To answer this question, more theoretical reactions were simulated with the kinetic constants reflecting no 'hand-off' activity (Fig. 11). As expected, methylation activity remained inhibited by RNA with increasing α. Altogether these results indicate that RNA inhibits PRC2's HMTase activity and will only act synergistically towards PRC2 when proximal to nucleosomes, facilitating the 'hand-off' to occur. This reconciles the antagonistic nature of RNA with its apparent involvement in targeting PRC2 to specific genes.

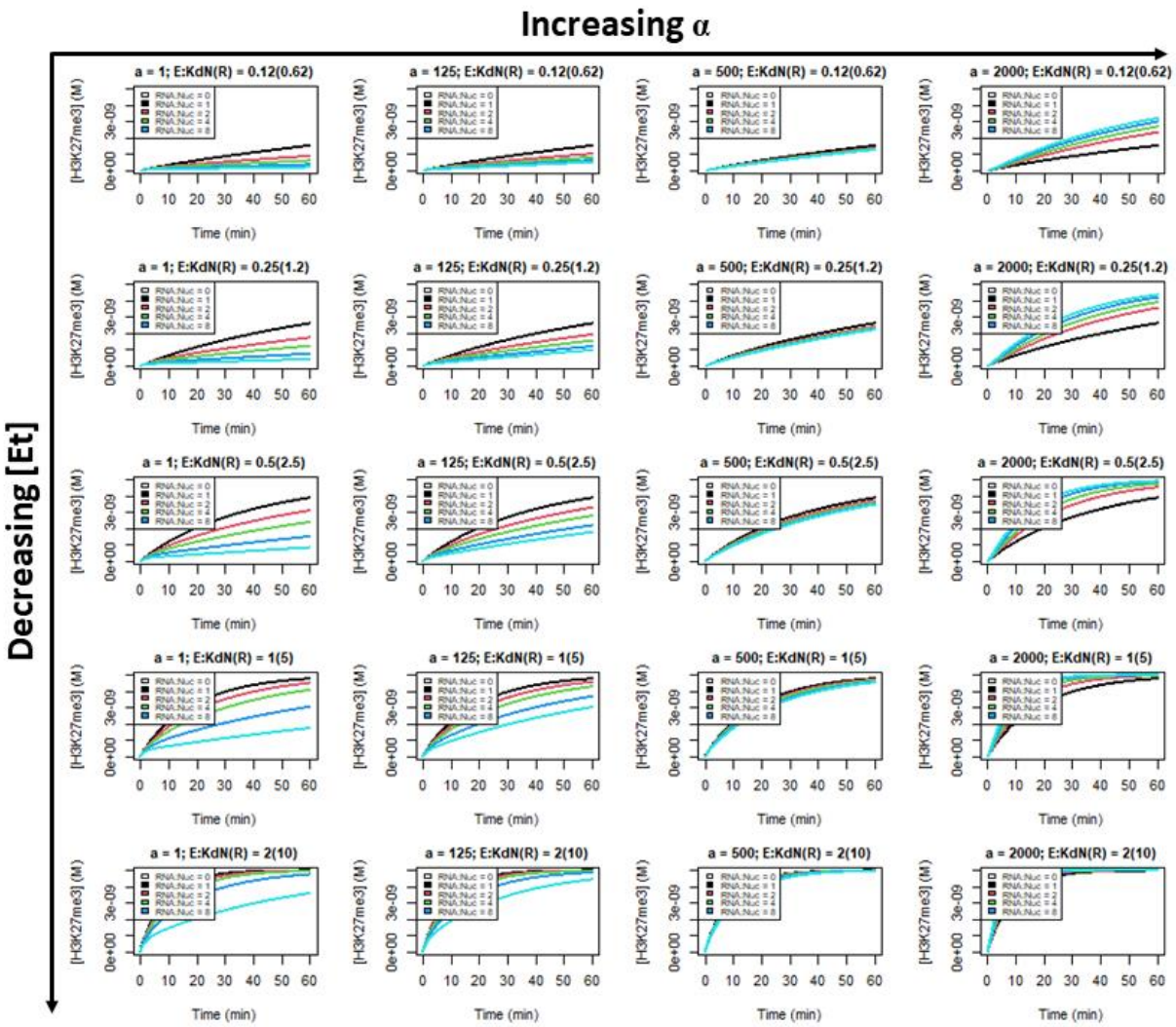

Figure 10. Theoretical reaction scheme shows RNA acting synergistically towards PRC2 when in close proximity to the nucleosome.

Using the previously derived rate constants, a theoretical reaction scheme was generated to simulate PRC2 HMTase activity for a range of proximity levels (α), PRC2 concentrations (E), and RNA-nucleosome ratios (RNA:Nuc).

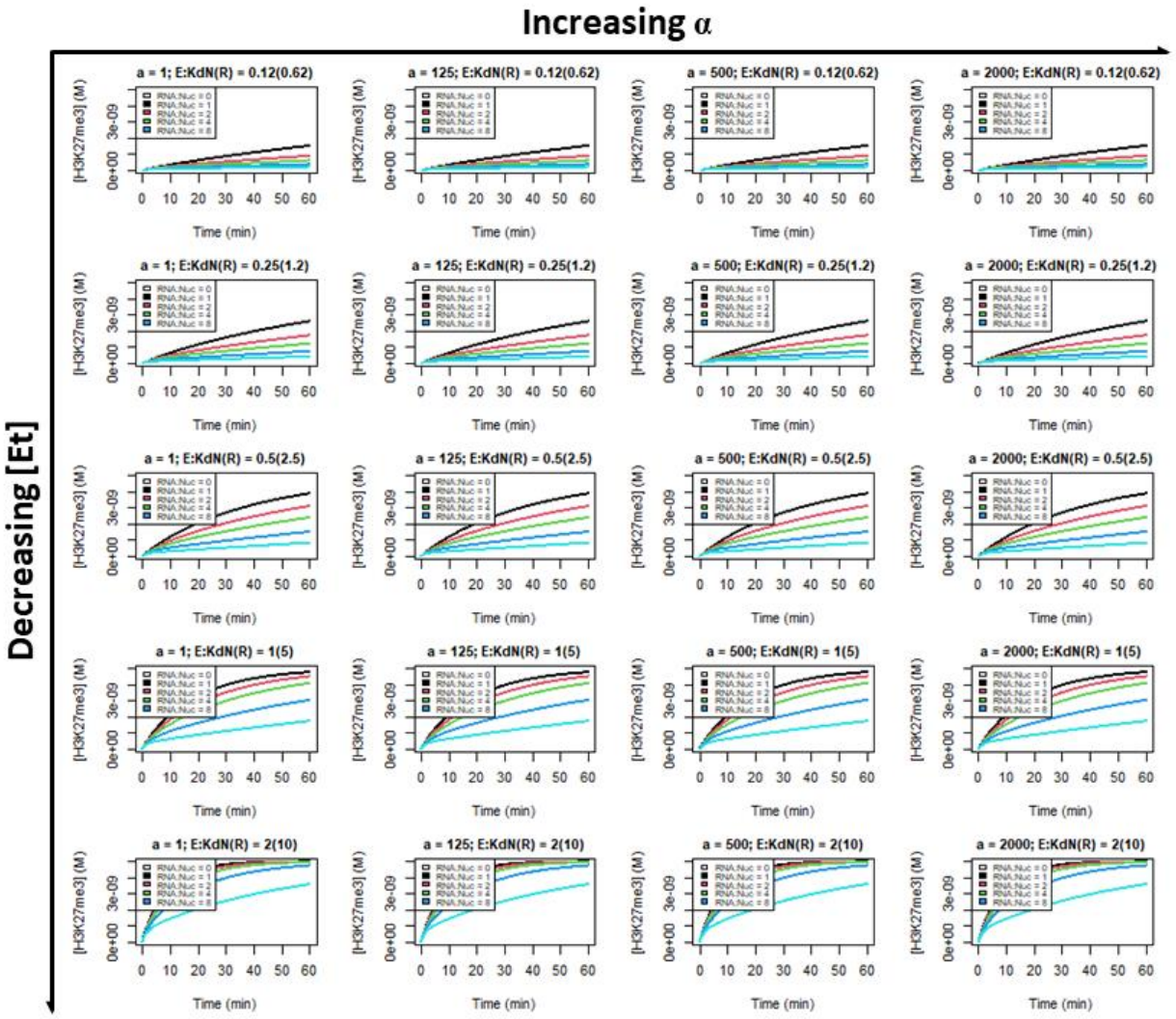

Figure 11. Theoretical reaction scheme shows RNA inhibiting PRC2 without 'hand-off' kinetics.

Using the previously derived rate constants, a theoretical reaction scheme was generated to simulate PRC2 HMTase activity for a range of proximity levels (α), PRC2 concentrations (E), and RNA-nucleosome ratios (RNA:Nuc). For these reactions, all kθ values (displacement-transfer constant) were set to 0 to mimic an environment with no 'hand-off' kinetics.

Discussion

Biological Implications

Through these experiments we have been able to show that PRC2 has the ability to 'hand-off' between G-quadruplex RNA and double-stranded CG-rich DNA. We demonstrated that DNA was more efficient at kicking off RNA from PRC2 than RNA was from DNA or itself. PRC2 has a strong association with RNA, so something needs to be stronger for it to leave RNA. The DNA species we tested were shown to have around the same (if not less) affinity as RNA, so there must be a biophysical reason as to how PRC2 can get onto chromatin efficiently instead of associating with a different RNA. DNA being a more effective displacer would allow for RNA to associate with PRC2 until it reaches the target genes, whereupon the DNA could replace RNA, allowing for PRC2 to methylate the genes. DNA being more resistant to displacement supports this, as no other nucleotide species could efficiently displace the DNA from PRC2 before it finished methylation.

However, the experiments only proved the existence of a 'hand-off' mechanism *in vitro* with DNA. PRC2 methylates histones, so seeing this mechanism happen with nucleosomes would be more biologically relevant than free DNA. To investigate this further, the theoretical nucleosome data showed that RNA was able to simultaneously have an antagonistic and synergistic effect on PRC2 depending on the distance between the RNA and the nucleosome (Fig. 10, 11). This reconciled the *in vitro* and *in vivo* results of RNA inhibiting PRC2 while being necessary for its recruitment. Altogether these results provided direct evidence for a proposed mechanism of how PRC2 is recruited to its target genetic loci and transferred onto the nucleosome from the nascent RNA (Fig. 13).

One lingering question presented by this data is why the 'hand-off' kinetics of DNA displacing RNA is stronger than RNA displacing other species. Since the G-quad RNA and dsDNA species tested had relatively similar affinities to PRC2 (under tested buffer conditions), it is interesting how the 'hand-off' kinetics differ in favor of DNA. These competing ligands share protein-polynucleotide interactions, so for one species there could be additional interactions with the enzyme. The salt-dependency data confirms this, with the dsDNA species showing different affinities to PRC2 with different salt concentrations. The lower KCl concentration showed high affinity to both DNA and RNA, but as the KCl concentration got higher, the affinity dropped significantly for the DNA and not the RNA species. This implies that DNA has additional ionic contacts with PRC2 that are not shared with RNA. These ionic contacts allow for DNA to have a better hold on PRC2, so it is not as easily displaced by RNA. Without these contacts, RNA can then be easily displaced by DNA, confirming the differing kinetics, and matching with the proposed model with the end goal of PRC2 on the nucleosome to deposit the methyl marks.

Future Directions

One possibly interesting avenue could be to investigate the unstructured RNA species more with its relationship to PRC2. The rGA-40 data had different results than we were expecting, showing a high affinity to PRC2 rivaling the G-quad RNA species. Since the rGA-40 species is unstructured RNA, it should have a lesser affinity than the G-quadruplex-forming rG4-20 species because PRC2 has been shown to associate with G-quadruplex structures with a higher affinity. One possibility is that rGA-40 could be forming a secondary structure that could have a higher affinity to PRC2 than unstructured RNA would. To test if the rGA-40 species was forming a secondary structure of any kind, it was run on a polyacrylamide gel alongside rG4-20,

but the results were inconclusive (data not shown). The rGA-40 was also investigated with different fluorescent tags (Alexa tag, Cy5) to see if the [FAM] tag was influencing the affinity. There was a difference in the affinity to PRC2 with different fluorescent tags (data not shown) that was not seen with the G-quad species, so this could be contributing to the unexpected affinity. I think it could be interesting to investigate this further to see how the tag could be helping affinity, and if there is anything else about the rGA-40 species that would help its affinity to PRC2.

It would be greatly beneficial to study this 'hand-off' model of kinetics in an environment that more closely resembles the cell. The reaction schemes for nucleosome:RNA competition look promising for this effect *in vivo,* but this data is only theoretical. If an experiment could be done using nucleosomes instead of dsDNA for these competition experiments, it would be a step in the right direction to investigate this further. Wayne Hemphill is currently working to get nucleosome species to use for these experiments. As the results come in, they will hopefully solidify that this effect is still seen with full nucleosomes rather than just a free DNA.

Although this would be a good first step, it would not be enough to prove this mechanism is viable in vivo. In order to fully test the proposed model, a construct with the nascent RNA attached to RNA polymerase upstream of a nucleosome array to which the PRC2 could deposit its methyl marks would be needed. At the moment an experiment like this would be challenging to conduct as this construct is difficult to make. If this is conducted in vitro, this would also not consider other environmental factors that could make a difference in the cell. At the moment this is highly unlikely to happen, but hopefully in the future this could be done.

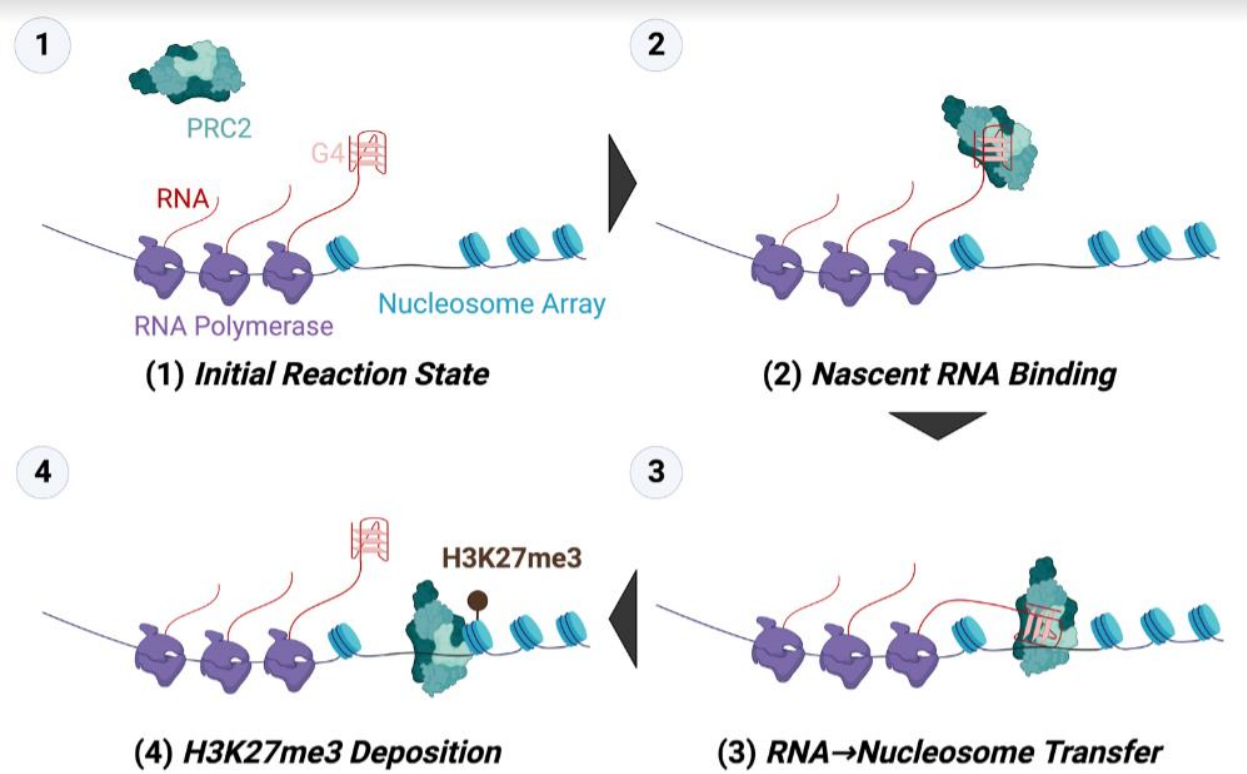

Figure 13. Proposed mechanism of PRC2:RNA:nucleosome transfer *in vivo*.

A G-quadruplex RNA would be attached to an RNA Polymerase upstream of the target nucleosome array (1). PRC2 would associate with the nascent G-quad RNA and bring the PRC2 closer to the target gene loci (2). After PRC2 has been transferred to the nucleosome through the 'hand-off' kinetics of transfer (3), it can begin methylating the histone (4).

Materials and Methods

Preparation of oligos

All oligos were ordered from IDT. A key of the name and sequence of each species is provided (Table 2). All dsDNA constructs were ordered as complementary single-stranded species and annealed to make double-stranded DNA. To anneal, oligos were mixed at 5 µM each in an annealing buffer (50 mM tris pH 7.5, 200 mM NaCl) and put through a pre-set thermocycler program (95°C for 10-min, decrease to 4°C at a rate of 0.5°C/min, suspend at 95°C). Annealing was confirmed with a native-PAGE gel. 100 µM and 100 nM stocks of each oligo were made, and concentrations were confirmed using spectroscopy with extinction coefficients provided by IDT.

Protein purification

Sf9 cells were infected with 5mer PRC2 short form (short isoform of AEBP2) by Anne Gooding. The PRC2 was prepared for use in experiments by Wayne Hemphill by lysing and clarifying the cell paste containing the expressed protein, then purified by amylose column chromatography, MBP-tag cleavage, heparin column chromatography, and size-exclusion column chromatography.

Buffer preparation

Binding buffers were created using a standard buffer recipe [50 mM Tris (pH 7.5), 2.5 mM $MgCl_2$, 0.1 mM $ZnCl_2$, 0.1 mg/mL BSA, 5% v/v glycerol, 2 mM 2-mercaptoethanol] with

varying salt concentrations as referenced (Table 1). KCl concentration increased from 10 mM (low-salt buffer) to 200 (high-salt buffer) mM for all experiments as indicated by buffer name.

FP-Based K_d determination experiments

Reaction mix was prepared with 5 nM prey molecule ([FAM]-labeled construct) in 1X Binding Buffer with indicated salt concentration (Table 1). 2 or 4 reaction replicates of each reaction per protein concentration were calculated and pipetted into the wells of a 384-well black microplate (Corning #3575) with 36 µL of the respective reaction mix in each well, with a row of 4 wells containing 40 µL of the binding buffer. The protein was prepared at 10 µM with 11 sequential concentrations of 2-fold serial dilutions in the binding buffer. The plated reaction mixes and protein dilutions were incubated separately at room temperature for 30 minutes. The binding reactions were initiated by addition of 4 µL of the diluted protein, then fluorescence polarization readings were taken for 30 min in 30 s intervals with a TECAN Spark microplate reader (Excitation setting = 481 ± 20 nm, Emission setting = 526 ± 20 nm). Raw parallel and perpendicular readings were analyzed in RStudio (v.4.1.1) using the FPalyze function (FPalyze v1.3.0 package) by taking the average last 10 data points for each reaction and plotting it as a function of protein concentration. The data was regressed using Eq. 2 to calculate the apparent K_d for the protein-polynucleotide interaction. Binding curves were then graphed together according to the appropriate comparison.

FP-Based Competition dissociation experiments

Reaction mix was prepared with 5 nM prey molecule ([FAM]-labeled construct) and 10uM PRC2 in 1X Binding Buffer with indicated salt concentration (Table 1). Four reaction replicates of each reaction per protein concentration were calculated and pipetted into the wells of a 384-well black microplate (Corning #3575) with 36 µL of the respective reaction mix in each well, with a row of 4 wells containing 40 µL of the binding buffer. The decoy molecule (unlabeled construct) was prepared at 1 µM with 11 sequential concentrations of 2-fold serial dilutions in the binding buffer. The plated reaction mixes and protein dilutions were incubated separately at the indicated temperature/time (4°C/90min or 25°C/30min) to achieve binding equilibrium between the prey and protein. The dissociation reactions were initiated by addition of 4 µL of the diluted decoy molecule, then fluorescence polarization readings were taken for 120 min in 30 s intervals with a TECAN Spark microplate reader (Excitation setting = 481 ± 20 nm, Emission setting = 526 ± 20 nm). Raw parallel and perpendicular readings were analyzed in RStudio (v.4.1.1) using the FPalyze function (FPalyze v1.3.0 package) by normalizing each reaction's polarization data to the maximum and minimum polarization across all reactions, then fitting each normalized reaction with an exponential dissociative function (Eq. 3.1) to determine k_{off} (Eq. 3.2) which was plotted as a function of decoy concentration. The plots were regressed using Eq. 4.1 and 4.2 to determine the best-fitting regression model.

Theoretical reaction schemes

The theoretical reaction schemes were generated using a custom script in RStudio (v.4.1.1) by Wayne Hemphill. Rate constants and initial conditions not provided were calculated using Eq. 7, and the differential equations (Eq. 5) were solved numerically.

Equations

All equations were calculated by Wayne Hemphill and utilized to analyze the data in this paper.

Eq. 1.1-10 define the reaction scheme of FP data. E is the protein PRC2, P is prey, D is decoy. This series of equations provide the rates of change for the indicated reactants as a function of time.

(Eq. 1.1) $[E]_t' = k_{-1P}\,[EP]_t + k_{-1D}\,[ED]_t - k_{1P}\,[E]_t\,[P]_t - k_{1D}\,[E]_t\,[D]_t$

(Eq. 1.2) $[P]_t' = k_{-1P}\,[EP]_t + k_{\theta D}\,[EP]_t\,[D]_t - k_{1P}\,[E]_t\,[P]_t - k_{\theta P}\,[ED]_t\,[P]_t$

(Eq. 1.3) $[D]_t' = k_{-1D}\,[ED]_t + k_{\theta P}\,[ED]_t\,[P]_t - k_{1D}\,[E]_t\,[D]_t - k_{\theta D}\,[EP]_t\,[D]_t$

(Eq. 1.4) $[EP]_t' = k_{1P}\,[E]_t\,[P]_t + k_{\theta P}\,[ED]_t\,[P]_t - k_{-1P}\,[EP]_t - k_{\theta D}\,[EP]_t\,[D]_t$

(Eq. 1.5) $[ED]_t' = k_{1D}\,[E]_t\,[D]_t + k_{\theta D}\,[EP]_t\,[D]_t - k_{-1D}\,[ED]_t - k_{\theta P}\,[ED]_t\,[P]_t$

(Eq. 1.6) $[E_T] = [E] + [EP] + [ED]$

(Eq. 1.7) $[P_T] = [P] + [EP]$

(Eq. 1.8) $[D_T] = [D] + [ED]$

(Eq. 1.9) $K_{dP} = \frac{k_{-1P}}{k_{1P}}$

(Eq. 1.10) $K_{dD} = \frac{k_{-1D}}{k_{1D}}$

Eq. 2 defines the exponential fit of each dissociation reaction. P_E is polarization at a given $[E_T]$, P_{max} is the maximum polarization, P_{min} is the minimum polarization, $[E_T]$ is the total protein concentration, and K_d^{app} is the apparent dissociation constant.

(Eq. 2) $P_E = (P_{max} - P_{min}) \frac{[E_T]}{[E_T] + K_d^{app}} + P_{min}$

Eq. 3 defines the observed dissociation rate k_{off}^{obs}. N_t is the relative polarization at a given time, N_{min} is the minimum relative polarization, and λ is the decay rate constant.

(Eq. 3.1) $N_t = (1 - N_{min}) e^{-\lambda t} + N_{min}$

(Eq. 3.2) $k_{off}^{obs} = (1 - N_{min}) \lambda$

Eq. 4 defines the regression fit lines of both the hand-off and classic models for competition data. The notation is the same as Eq. 1 with extra tuning parameters α and β.

(Eq. 4.1) $\frac{-[EP]_0}{[EP]_0} = k_{off}^{obs} \approx \frac{[D_T]^\beta}{\alpha^\beta + [D_T]^\beta} k_{-1P} + k_{\theta D} [D]_t$

(Eq. 4.2) $\frac{-[EP]_0}{[EP]_0} = k_{off}^{obs} \approx \frac{[D_T]^\beta}{\alpha^\beta + [D_T]^\beta} k_{-1P}$

Eq. 5 defines the rates of change for the indicated reactants as a function of time in the theoretical data. E is the protein PRC2, R is RNA, N is nucleosomes, and Nm is methylated nucleosomes.

(Eq. 5.1) $[E]_t' = k_{-1N} ([EN]_t + [EN^m]_t) + k_{-1R} [ER]_t - [E]_t (k_{1N} ([N]_t + [N^m]_t) + k_{1R} [R]_t)$

(Eq. 5.2) $[N]_t' = [EN]_t (k_{-1N} + k_{\theta NN} [N^m]_t + \alpha k_{\theta R} [R]_t) - [N]_t (k_{1N} [E]_t + k_{\theta NN} [EN^m]_t + \alpha k_{\theta N} [ER]_t)$

(Eq. 5.3) $[R]_t' = [ER]_t (k_{-1R} + \alpha k_{\theta N} ([N]_t + [N^m]_t)) - [R]_t (k_{1R} [E]_t + \alpha k_{\theta N} ([EN]_t + [EN^m]_t))$

(Eq. 5.4) $[N^m]_t' = [EN^m]_t (k_{\theta NN} [N]_t + \alpha k_{\theta R} [R]_t + k_{-1N}) - [N^m]_t (k_{\theta NN} [EN]_t + k_{-1N} [E]t + \alpha k_{\theta N} [ER]_t)$

(Eq. 5.5) $[EN]_t' = [N]_t (k_{1N} [E]_t + k_{\theta NN} [EN^m]_t + \alpha k_{\theta N} [ER]_t) - [EN]_t (k_{cat} + k_{-1N} + k_{\theta NN} [N^m]_t + \alpha k_{\theta R} [R]_t)$

(Eq. 5.6) $[ER]_t' = [R]_t (k_{1R} [E]_t + \alpha k_{\theta R} ([EN]_t + [EN^m]_t)) - [ER]_t (\alpha k_{\theta N} ([N]_t + [N^m]_t) + k_{-1R})$

(Eq. 5.7) $[EN^m]_t' = k_{cat} [EN]_t + [N^m]_t (k_{\theta NN} [EN]_t + k_{1N} [E]t + \alpha k_{\theta N} [ER]_t) - [EN^m]_t (k_{\theta NN} [N]_t + \alpha k_{\theta R} [R]_t + k_{-1N})$

(Eq. 5.8) $[E_T] = [E] + [EN] + [ER] + [EN^m]$

(Eq. 5.9) $[R_T] = [R] + [ER]$

(Eq. 5.10) $[N_T] = [N] + [N^m] + [EN] + [EN^m]$

(Eq. 5.11) $[m_T] = [N^m] + [EN^m]$

Eq. 7 is a continuation of Eq. 5 to calculate the theoretical data.

(Eq. 7.1) $k_1 = \frac{k_{-1}}{K_d}$

(Eq. 7.2) $[E]_0 = [E_T]$

(Eq. 7.3) $[R]_0 = [R_T]$

(Eq. 7.4) $[N]_0 = [N_T]$

(Eq. 7.5) $[N^m]_0 = [EN]_0 = [ER]_0 = [EN^m]_0 = 0$

Acknowledgements

I would like to thank the members of the Cech lab for all the help and support they have given me while I have worked on this project:

Karen Goodrich, Arthur Zaug, Laura Konyha, Jiarui Song, Linnea Inga Jansson-Fritzberg, Kaitlin Johnson, Liyi Cheng, Jessica Song, Camila Sousa

I would like to thank Anne Gooding for her help in the preparation of the protein used throughout this project.

I would also like to acknowledge my Honors Thesis Committee members:

Dr. Thomas Cech, Dr. Christy Fillman, Dr. Jihye Park

Finally, I would like to acknowledge Dr. Thomas Cech for providing me with the opportunity to work in this lab, and especially Wayne Hemphill for guiding me through this project and providing equations and experimental help.

References

Beltran, M. et al. (2016). The interaction of PRC2 with RNA or chromatin is mutually antagonistic. Genome research, 26(7), 896–907. https://doi.org/10.1101/gr.197632.115

Beltran, M. et al. (2019). G-tract RNA removes Polycomb Repressive Complex 2 from genes. Nature Structural & Molecular Biology, 26, 899–909. https://doi.org/10.1038/s41594019-0293-z

Betancur J., Tomari Y. (2015) Cryptic RNA-binding by PRC2 components EZH2 and SUZ12. RNA Biology, 12(9), 959-65. https://doi.org/10.1080/15476286.2015.1069463

Birve, A. et al. (2001). Su(z)12, a novel Drosophila Polycomb group gene that is conserved in vertebrates and plants. Development (Cambridge, England), 128(17), 3371–3379. https://doi.org/10.1242/dev.128.17.3371

Cao, R. et al. (2002). Role of histone H3 lysine 27 methylation in Polycomb-group silencing. Science (New York, N.Y.), 298(5595), 1039–1043. https://doi.org/10.1126/science.1076997

Cifuentes-Rojas, C. et al. (2014). Regulatory interactions between RNA and Polycomb repressive complex 2. Molecular cell, 55(2), 171–185. https://doi.org/10.1016/j.molcel.2014.05.009

Czermin, B. et al. (2002). Drosophila enhancer of Zeste/ESC complexes have a histone H3

methyltransferase activity that marks chromosomal Polycomb sites. Cell, 111(2), 185-196. https://doi.org/10.1016/s0092-8674(02)00975-3

Dandliker W. B. & de Saussure V. A. (1970). Fluorescence polarization in immunochemistry. Immunochemistry, 7, 799-828. Pergamon Press.

Davidovich, C., & Cech, T. R. (2015). The recruitment of chromatin modifiers by long noncoding RNAs: lessons from PRC2. RNA (New York, N.Y.), 21(12), 2007–2022. https://doi.org/10.1261/rna.053918.115

Davidovich, C. et al. (2013). Promiscuous RNA binding by Polycomb repressive complex 2. Nature structural & molecular biology, 20(11), 1250–1257. https://doi.org/10.1038/nsmb.2679

Davidovich, C. et al. (2015). Toward a consensus on the binding specificity and promiscuity of PRC2 for RNA. Molecular cell, 57(3), 552–558. https://doi.org/10.1016/j.molcel.2014.12.017

Di Croce, L., & Helin, K. (2013). Transcriptional regulation by Polycomb group proteins. Nature structural & molecular biology, 20(10), 1147–1155. https://doi.org/10.1038/nsmb.2669

Grijzenhout, A. et al. (2016). Functional analysis of AEBP2, a PRC2 Polycomb protein, reveals a Trithorax phenotype in embryonic development and in ESCs. Development (Cambridge, England), 143(15), 2716–2723. https://doi.org/10.1242/dev.123935

Hendrickson, D. et al. (2016). Widespread RNA binding by chromatin-associated proteins. Genome Biology, 17, 28. https://doi.org/10.1186/s13059-016-0878-3

Kaneko, S. et al. (2013). PRC2 binds active promoters and contacts nascent RNAs in embryonic stem cells. Nature Structural & Molecular Biology, 20, 1258–1264. https://doi.org/10.1038/nsmb.2700

Kaneko, S. et al. (2014). Nascent RNA interaction keeps PRC2 activity poised and in check. Genes & development, 28(18), 1983–1988. https://doi.org/10.1101/gad.247940.114

Khalil, A. M. et al. (2009). Many human large intergenic noncoding RNAs associate with chromatin-modifying complexes and affect gene expression. PNAS, 106, 11667–11672. https://doi.org/10.1073/pnas.0904715106

Kim, H. et al. (2015). AEBP2 as a transcriptional activator and its role in cell migration. Genomics, 105(2), 108–115. https://doi.org/10.1016/j.ygeno.2014.11.007

Kuzmichev, A. et al. (2002). Histone methyltransferase activity associated with a human multiprotein complex containing the Enhancer of Zeste protein. Genes & development, 16(22), 2893–2905. https://doi.org/10.1101/gad.1035902

Long, Y. et al. (2017). Conserved RNA-binding specificity of polycomb repressive complex 2 is achieved by dispersed amino acid patches in EZH2. Elife, 6. https://doi.org/10.7554%2FeLife.31558

Long, Y. et al. (2020). RNA is essential for PRC2 chromatin occupancy and function in human pluripotent stem cells. Nature Genetics, 52, 931–938. https://doi.org/10.1038/s41588020-0662-x

Margueron, R., & Reinberg, D. (2011). The Polycomb complex PRC2 and its mark in life. Nature, 469(7330), 343–349. https://doi.org/10.1038/nature09784

Mendenhall, E. et al. (2010). GC-rich sequence elements recruit PRC2 in mammalian ES cells. PLoS Genetics, 6(12). https://doi.org/10.1371/journal.pgen.1001244

Müller, J. et al. (2002). Histone methyltransferase activity of a Drosophila Polycomb group repressor complex. Cell, 111(2), 197–208. https://doi.org/10.1016/s0092-8674(02)0095

Nekrasov, M., Wild, B., & Müller, J. (2005). Nucleosome binding and histone methyltransferase activity of Drosophila PRC2. EMBO reports, 6(4), 348–353. https://doi.org/10.1038/sj.embor.7400376

Pandey, R. et al. (2008). Kcnq1ot1 antisense noncoding RNA mediates lineage-specific transcriptional silencing through chromatin-level regulation. Molecular cell, 32(2), 232 246. https://doi.org/10.1016/j.molcel.2008.08.022

Petracovici, A., & Bonasio, R. (2021). Distinct PRC2 subunits regulate maintenance and establishment of Polycomb repression during differentiation. Molecular cell, 81(12), 2625–2639. https://doi.org/10.1016/j.molcel.2021.03.038

Satijn, D. P. et al. (2001). The polycomb group protein EED interacts with YY1, and both proteins induce neural tissue in Xenopus embryos. Molecular and cellular biology, 21(4), 1360–1369. https://doi.org/10.1128/MCB.21.4.1360-1369.2001

Sigova, A. A. et al. (2015). Transcription factor trapping by RNA in gene regulatory elements. Science, 350, 978–981. https://doi.org/10.1126/science.aad3346

Simon, J. A., & Kingston, R. E. (2013). Occupying chromatin: Polycomb mechanisms for getting to genomic targets, stopping transcriptional traffic, and staying put. Molecular cell, 49(5), 808–824. https://doi.org/10.1016/j.molcel.2013.02.013

Wang, X. et al. (2017). Molecular analysis of PRC2 recruitment to DNA in chromatin and its inhibition by RNA. Nature Structural & Molecular Biology, 24(12), 1028–1038. https://doi.org/10.1038/nsmb.3487

Wang, X. et al. (2017). Targeting of Polycomb Repressive Complex 2 to RNA by Short Repeats of Consecutive Guanines. Molecular cell, 65(6), 1056–1067. https://doi.org/10.1016/j.molcel.2017.02.003

Wang, X. et al. (2019). C9orf72 and triplet repeat disorder RNAs: G-quadruplex formation, binding to PRC2 and implications for disease mechanisms. RNA, 25(8), 935-947. https://doi.org/10.1261/rna.071191.119

Wang, X. et al. (2019). Regulation of histone methylation by automethylation of PRC2. Genes &

Development, 33(19-20), 1416–1427. https://doi.org/10.1101/gad.328849.119

Yan, J., Dutta, B., Hee, Y. T., & Chng, W. J. (2019). Towards understanding of PRC2 binding to RNA. RNA biology, 16(2), 176–184. https://doi.org/10.1080/15476286.2019.1565283

Youmans, D. T. et al. (2018). Live-cell imaging reveals the dynamics of PRC2 and recruitment to chromatin by SUZ12-associated subunits. Genes & Development, 32(11-12). https://doi.org/10.1101/gad.311936.118

Zhang, Q. et al. (2019). RNA exploits an exposed regulatory site to inhibit the enzymatic activity of PRC2. Nature structural & molecular biology, 26(3), 237–247. https://doi.org/10.1038/s41594-019-0197-y

Zhao, Q. et al. (2020). Aptamer binding assays and molecular interaction studies using fluorescence anisotropy - A review. Analytica chimica acta, 1125, 267–278. https://doi.org/10.1016/j.aca.2020.05.061

Supplementary Information

Buffer ID	Buffer name	KCl concentration
BB6	Low	10 mM
BB1	Mid	25 mM
BB12	High	100 mM
BB13	Very High	200 mM

Table 1. Four Buffers were made at varying salt concentrations

All buffers were made using the buffer recipe referred to in the Materials and Methods section. The concentration of KCl in each buffer was varied and labeled as Low, Mid, High, and Very High depending on the concentration. BB1 was made with the same concentration used in the Wang et al. 2017 paper, 25mM KCl concentration. BB6 was made with a lower salt concentration for the binding experiments with DNA to maximize binding efficiency. BB12 and BB13 were made with higher KCl concentrations of 100mM and 200mM KCl respectively to be used in the salt-dependency experiments. Buffers are labeled on figure graphs by the 'Buffer Name'.

DNA Oligos Table

Name	IDT Seq	Sequence
dsCG-60	ds-d$(N)_{60}$	GAAGTGCCCGTGACGCGCGCGACGCCAGCCGACGAAGGCGGGACCCAGAGCGCGCGCCGT CTTCACGGGCACTGCGCGCGCTGCGGTCGGCTGCTTCCGCCCTGGGTCTCGCGCGCGGCA
dsCG-50	ds-d$(GCGTA)_{10}$	GCGTAGCGTAGCGTAGCGTAGCGTAGCGTAGCGTAGCGTAGCGTA CGCATCGCATCGCATCGCATCGCATCGCATCGCATCGCATCGCATCGCAT
ssCG-40	d$(GCGTA)_8$	GCGTAGCGTAGCGTAGCGTAGCGTAGCGTAGCGTA
ssG_4-20	d$(G_3A_2)_4$	GGGAAGGGAAGGGAAGGGAA
ssGA-40	d$(GA)_{20}$	GAGAGAGAGAGAGAGAGAGAGAGAGAGAGAGAGAGAGAGA
ssG_4-40	d$(GGAA)_{10}$	GGAAGGAAGGAAGGAAGGAAGGAAGGAAGGAAGGAAGGAA

RNA Oligos Table

Name	IDT Seq	Sequence
rG_4-20	r$(G_3A_2)_4$	GGGAAGGGAAGGGAAGGGAA
rGA-40	r$(GA)_{20}$	GAGAGAGAGAGAGAGAGAGAGAGAGAGAGAGAGAGAGAGA
rG_4-40	r$(GGAA)_{10}$	GGAAGGAAGGAAGGAAGGAAGGAAGGAAGGAAGGAAGGAA

Table 2. DNA and RNA Oligos

All oligos used in the paper are detailed in full sequence and naming forms in a separate table for DNA and RNA species. The 'Name' column details the naming convention by which each sequence is referred to in the paper. The sequences of the oligos are written out in full form from 5'→ 3' with both strands shown for the double-stranded DNA species. Each oligo species was ordered from IDT with and without a fluorescent [FAM] label. For the species with a fluorescent tag, they will be labeled in the paper with [F] denoting the placement of the tag on the species (on the 5' or 3' end).

a

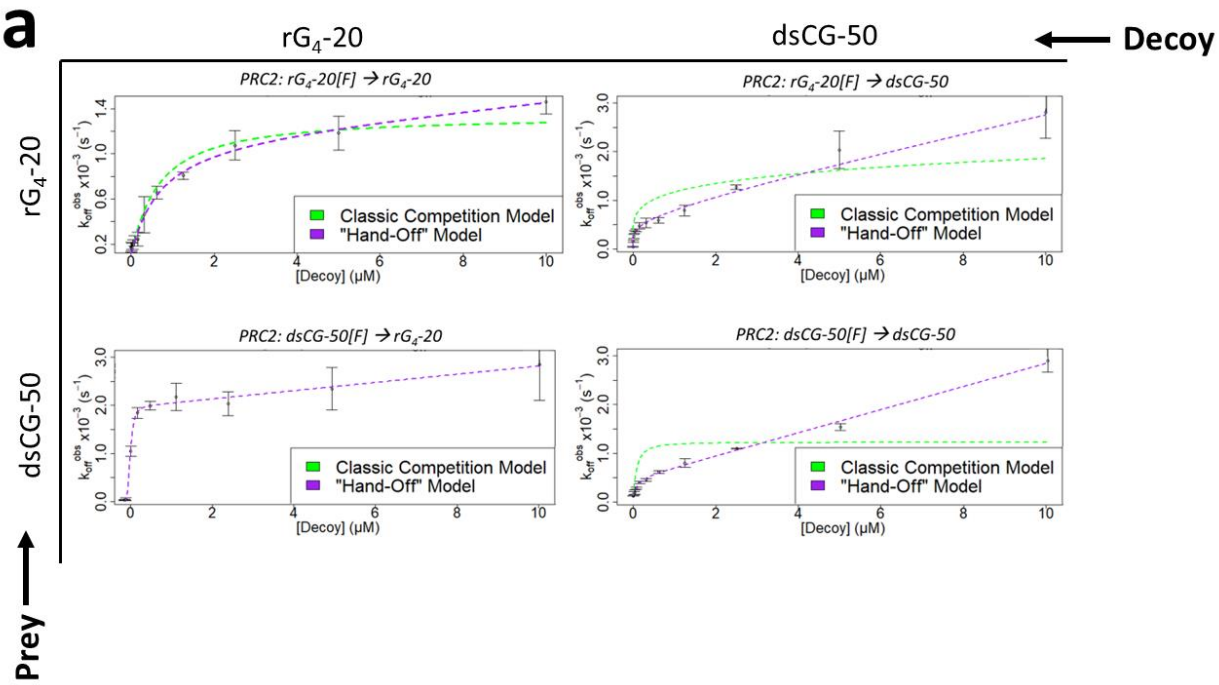

b

Prey	Decoy	k_{-1p} (s^{-1})	$k_{\theta D}$ ($M^{-1}s^{-1}$)
rG_4-20 [F]	rG_4-20	1.0 ± 0.01 ($x10^{-3}$)	37 ± 16
rG_4-20 [F]	dsCG-50	5.3 ± 2.0 ($x10^{-4}$)	150 ± 23
dsCG-50 [F]	rG_4-20	2.5 ± 0.3 ($x10^{-3}$)	87 ± 10
dsCG-50 [F]	dsCG-50	5.3 ± 2.3 ($x10^{-4}$)	150 ± 21

Supp. Figure 8. PRC2 did not exhibit the same "Hand-Off" Kinetics for Competition Dissociation with dsCG-50 and G-quadruplex RNA.

(a) FP-Competition experiments were run with combinations of G-quad RNA and dsCG-50 DNA as prey and decoy as labeled. All experiments (excluding RNA → RNA which was run at 4C) were run at room temperature 25C with mid-salt buffer conditions.

(b) The competition dissociation values calculated by regression statistics were similar to the CG-60 DNA results.

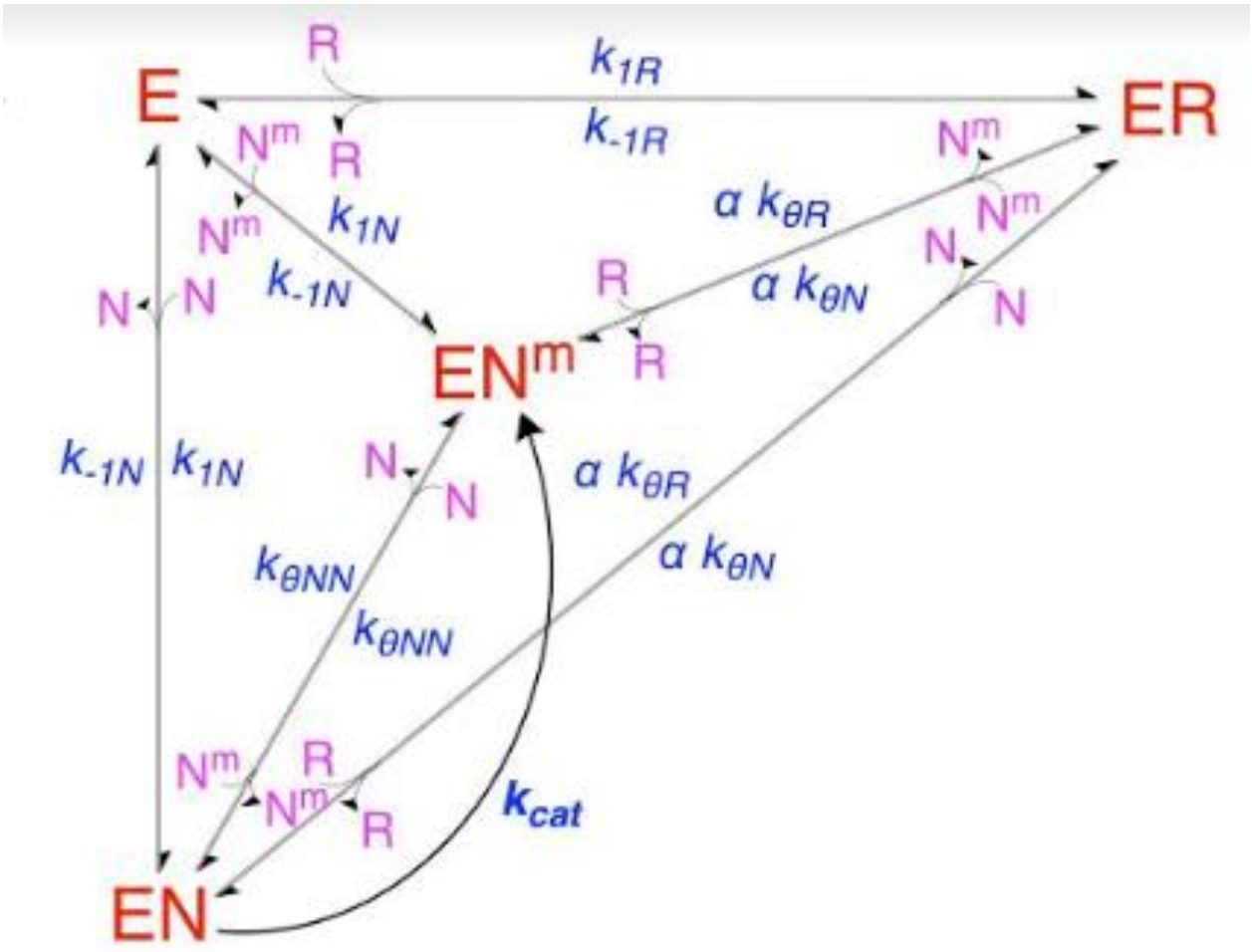

Supp. Figure 9. Theoretical reaction scheme for 'hand-off' kinetics *in vivo.*

A reaction scheme was made showing the association and dissociation rate constants for the kinetic transfer of RNA and nucleosomes, methylated and unmethylated, with PRC2. All values are listed in Eq. 5 and Eq. 7.